Cable bacteria generate a firewall against euxinia in seasonally hypoxic basins

Dorina Seitaj[a,1], Regina Schauer[b], Fatimah Sulu-Gambari[c], Silvia Hidalgo-Martinez[a], Sairah Y. Malkin[d,2], Laurine D. W. Burdorf[a], Caroline P. Slomp[c], and Filip J. R. Meysman[a,d,1]

[a]Department of Ecosystem Studies, Royal Netherlands Institute for Sea Research, 4401 NT Yerseke, The Netherlands; [b]Center for Microbiology, Department of Bioscience, Aarhus University, 8000 Aarhus, Denmark; [c]Department of Earth Sciences–Geochemistry, Faculty of Geosciences, Utrecht University, 3584 CD Utrecht, The Netherlands; and [d]Department of Analytical, Environmental, and Geochemistry, Vrije Universiteit Brussel, 1050 Brussels, Belgium

Edited by Donald E. Canfield, Institute of Biology and Nordic Center for Earth Evolution, University of Southern Denmark, Odense M, Denmark, and approved September 10, 2015 (received for review May 23, 2015)

Seasonal oxygen depletion (hypoxia) in coastal bottom waters can lead to the release and persistence of free sulfide (euxinia), which is highly detrimental to marine life. Although coastal hypoxia is relatively common, reports of euxinia are less frequent, which suggests that certain environmental controls can delay the onset of euxinia. However, these controls and their prevalence are poorly understood. Here we present field observations from a seasonally hypoxic marine basin (Grevelingen, The Netherlands), which suggest that the activity of cable bacteria, a recently discovered group of sulfur-oxidizing microorganisms inducing long-distance electron transport, can delay the onset of euxinia in coastal waters. Our results reveal a remarkable seasonal succession of sulfur cycling pathways, which was observed over multiple years. Cable bacteria dominate the sediment geochemistry in winter, whereas, after the summer hypoxia, *Beggiatoaceae* mats colonize the sediment. The specific electrogenic metabolism of cable bacteria generates a large buffer of sedimentary iron oxides before the onset of summer hypoxia, which captures free sulfide in the surface sediment, thus likely preventing the development of bottom water euxinia. As cable bacteria are present in many seasonally hypoxic systems, this euxinia-preventing firewall mechanism could be widely active, and may explain why euxinia is relatively infrequently observed in the coastal ocean.

sediment biogeochemistry | cable bacteria | coastal hypoxia | sulfur cycling | microbial competition

The depletion of oxygen in bottom waters (hypoxia) is a naturally recurring phenomenon in some coastal systems (1), such as basins with restricted water circulation (2), and shelf regions subject to strong nutrient upwelling (3). Alongside this natural hypoxia, there is evidence for a global increase in the frequency, extent, intensity, and duration of coastal hypoxia, which is linked to an increased anthropogenic input of nutrients into the coastal ocean in combination with climate change (1, 4–6). The development of bottom water hypoxia has major consequences for the functioning of coastal ecosystems, sometimes leading to the formation of "dead zones" characterized by a complete absence of benthic fauna and fish. Areas sensitive to hypoxia are typically major fishing grounds, so the resulting economic and biodiversity losses make the global expansion of coastal hypoxia a subject of growing concern (7, 8).

The ecosystem impacts of coastal hypoxia are particularly amplified when bottom water oxygen depletion progresses to a critical transition, termed euxinia, when free sulfide escapes from the sediment and accumulates in the bottom water (9). Even low levels of free sulfide are toxic to metazoan life, and therefore euxinia can induce mass mortality events, even among highly motile fauna like fish and large crustaceans (9–11). Although strong oxygen depletion, or even a complete removal of oxygen (anoxia), is often reported, concomitant reports of euxinia in coastal bottom waters are much scarcer. This suggests that certain sedimentary processes delay the onset of euxinia relative to anoxia, but, at present, the environmental controls on the timing and formation of coastal euxinia are poorly understood.

Here we document a microbial mechanism that can delay or even prevent the development of euxinia in seasonally hypoxic basins. The mechanism is based on the metabolic activity of a newly discovered type of electrogenic microorganism, named cable bacteria (*Desulfobulbaceae,* Deltaproteobacteria), which are capable of inducing electrical currents over centimeter-scale distances in the sediment (12, 13). Cable bacteria have recently been suggested to be abundant in seasonally hypoxic coastal systems (14), but their impact on the biogeochemical cycling in these systems is unknown. These filamentous bacteria possess a unique respiratory metabolism in which the oxidative removal of sulfide in deeper sediment layers is electrically coupled to the reductive consumption of oxygen just below the sediment–water interface (12), a process referred to as electrogenic sulfur oxidation (e-SOx) (15). In laboratory experiments, e-SOx has been shown to exert a strong impact on sedimentary iron and sulfur cycling, leading to a conversion of iron sulfides into iron oxides (16). Here we demonstrate that the same interconversion process of iron minerals occurs in the sediments of a seasonally hypoxic marine basin, and that the large pool of iron oxides can act as a "firewall," which can substantially delay the development of euxinia.

Significance

Seasonal hypoxia is increasing in coastal areas worldwide, as more nutrients are delivered to the coastal ocean and water temperatures are rising due to climate change. Hypoxia reaches a particularly harmful stage when sulfide, which is highly toxic for marine life, is released to the bottom water. Here, we document a natural microbial mechanism that counteracts the release of free sulfide, thus preventing the most adverse stage of seasonal hypoxia. Electricity-generating cable bacteria produce a large pool of oxidized sedimentary iron minerals, which efficiently bind free sulfide. As cable bacteria are likely abundant in many seasonally hypoxic basins worldwide, their "firewall" mechanism may be widespread.

Author contributions: D.S., F.S.-G., C.P.S., and F.J.R.M. designed research; D.S., R.S., F.S.-G., S.H.-M., and L.D.W.B. performed research; D.S., S.Y.M., and F.J.R.M. analyzed data; D.S. and F.J.R.M. wrote the paper; and F.J.R.M. coordinated sampling campaigns.

The authors declare no conflict of interest.

This article is a PNAS Direct Submission.

Freely available online through the PNAS open access option.

[1]To whom correspondence may be addressed. Email: dorina.seitaj@nioz.nl or filip.meysman@nioz.nl.

[2]Present address: Horn Point Laboratory, University of Maryland Center for Environmental Science, Cambridge, MD 21613.

This article contains supporting information online at www.pnas.org/lookup/suppl/doi:10.1073/pnas.1510152112/-/DCSupplemental.

Results and Discussion

Response of Pore Water Geochemistry to Seasonal Oxygenation. The sediment geochemistry, sediment fauna, and sedimentary microbial communities were surveyed in Marine Lake Grevelingen (MLG, The Netherlands), a coastal water body (salinity ~30) with restricted water exchange with the open North Sea. Over the last decade, MLG has experienced a regular pattern of summer stratification and bottom water oxygen depletion (Fig. S1*A*), which was also observed in monthly sampling campaigns performed throughout 2012 (Fig. S1*B*). Bottom water oxygen concentrations (Winkler method; Fig. 1*A*) were near air saturation in winter and early spring, started to decline in April at the onset of stratification, became hypoxic (O_2 < 63 μM) by the end of May, and declined below the detection limit in August (O_2 <1 μM; anoxia). In September, the overturning of the water column resulted in a reoxygenation of the bottom water.

Due to sediment focusing, the deeper basins in MLG experience a strong accumulation (~2 cm·y^{-1}) of dark, organic-rich, fine-grained sediment (14). Free sulfide ($\Sigma H_2S = [HS^-] + [H_2S]$) accumulates in the pore water to high levels (~2 mM at 10 cm depth; Fig. S2), suggesting that intensive organic mineralization takes place in the surface sediment and that sulfate reduction is the major mineralization pathway (estimated to be ~30 mmol S·m^{-2}·d^{-1} in August; *Supporting Information*). The burial of pyrite and iron sulfides only scavenges ~39% of the sulfide production (*Supporting Information*), and bottom water concentrations of nitrate (the alternative electron acceptor) are generally low in MLG (Fig. S1*B*). Accordingly, oxygen appears to be the main electron acceptor for the oxidation of the large amount of free sulfide that is produced by sulfate reduction (*Supporting Information*).

Nevertheless, microsensor profiling revealed that O_2 and H_2S were almost never in direct contact in the pore water, as a well-developed suboxic zone was present throughout most of the year (Fig. 1*B*), i.e., a distinct sediment horizon where neither O_2 nor ΣH_2S were present in detectable concentrations. This suboxic zone was widest in the first part of the year (annual maximum of 17.6 ± 4.6 mm in April), and its width decreased in a stepwise fashion by ~50% in late spring (May, 8.9 ± 2.1; June, 7.0 ± 5.2 mm). When the oxygen saturation of the bottom water dropped below 11% (corresponding to 29 μmol·L^{-1}; July and August, Fig. 1*A*), the H_2S front started to move toward the sediment surface (Fig. 1*B*). However, free sulfide remained undetectable in bottom water samples collected at 2 m above the sediment surface during the stratified season (ΣH_2S < 0.2 μM; June, August). We additionally determined the ΣH_2S concentration in the overlying ~10 cm water of retrieved sediment cores, which confirmed that euxinia did not occur. After the overturning of the basin, the oxygen penetration depth (OPD) was small (0.7 ± 0.1 mm), indicative of strong oxygen uptake caused by reoxidation of reduced compounds. September was also the only month when the pore water depth profiles O_2 and H_2S showed an overlap (Fig. 1*B*), allowing the direct aerobic oxidation of sulfide ($H_2S + 2O_2 \rightarrow SO_4^{2-} + 2H^+$). A small suboxic zone reappeared in October (2.2 ± 0.9 mm) and gradually expanded (12.2 ± 1.6 mm in December).

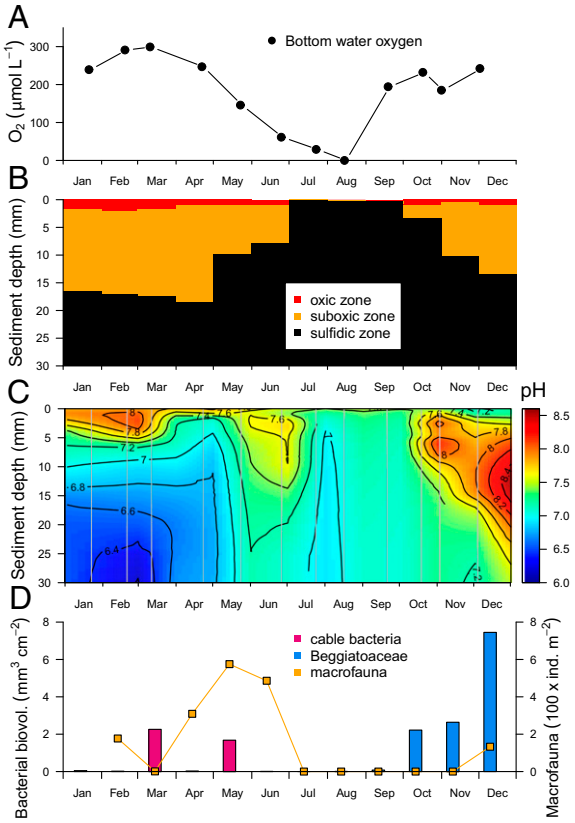

Fig. 1. (*A*) Oxygen concentration (in micromoles per liter) in the bottom water, measured at 1 m above the sediment surface throughout 2012. (*B*) Depth distribution of the oxic zone (red), suboxic zone (brown), and sulfidic zone (black) within the sediment throughout 2012. The data were obtained from microsensor measurements in intact sediment cores. (*C*) Pore water pH values in the upper 30 mm of the sediment measured monthly during 2012, in intact sediment cores. Gray lines indicate sampling dates. (*D*) Biovolume (in cubic millimeters per square centimeter) of cable bacteria (pink bars) and *Beggiatoaceae* (blue bars), and macrofauna abundance (100* individuals m^{-2}; orange line) recorded throughout 2012. Cable bacteria were enumerated in March, May, August, and November; *Beggiatoaceae* were counted monthly over the entire year 2012; macrofauna were determined monthly from February to December.

Mechanisms of Suboxic Zone Formation. To elucidate the underlying mechanisms of sulfide oxidation and suboxic zone formation, we developed a pH typology for three known mechanisms of aerobic sulfide oxidation (Fig. S3 and *Supporting Information*): (*i*) the e-SOx metabolism of the recently discovered cable bacteria (12, 13, 16); (*ii*) the cycling of iron between reduced and oxidized mineral forms, which is crucially dependent on solid-phase mixing (17, 18); and (*iii*) the respiratory metabolism of nitrate-accumulating *Beggiatoaceae* (19–22). Each of these three pathways is associated with a characteristic pH depth profile (Fig. 2, Fig. S3, and *Supporting Information*), which reveals when these mechanisms dominate the pore water geochemistry and are responsible for the formation of the suboxic zone (Fig. 1*C*). This pH typology predicted that e-SOx by cable bacteria was dominant from January to April, whereas metal cycling dominated in May and June, and respiration of nitrate-accumulating *Beggiatoaceae* created the suboxic zone in fall, after the ventilation and reoxygenation of the bottom water (Fig. 1*C*).

This temporal succession of sulfur oxidation pathways as predicted by the pH typology analysis was confirmed by direct microscopic observation of microbial and macrofaunal communities. Cable bacteria were enumerated on a seasonal basis by Fluorescence In Situ Hybridization (FISH), which revealed that cable bacteria were abundant in March and May (filament density 402–480 m·cm^{-2}; biovolume 1.8–2.5 mm^3·cm^{-2}), but remained below the detection limit in August and November (Fig. 1*D*). When present, cable bacteria were found throughout the upper 40 mm of the sediment, with the maximum density near the sediment surface, high densities in the suboxic zone, and low densities declining into the sulfidic zone (Fig. 2*A*, March). The filament diameter did not differ significantly (*t* test; $n = 15$, $P = 0.29$) between March (1.3 ± 0.3 μm) and May (1.2 ± 0.3 μm), suggesting that cable bacteria populations were phenotypically similar.

Quantitative microscopic enumeration of *Beggiatoaceae* was conducted each month (Fig. 1*D*), and showed low densities in spring (biovolume B: 0.02–0.05 mm^3·cm^{-2}), when only a few filaments were found dispersed throughout the upper 2 cm of sediment, and a

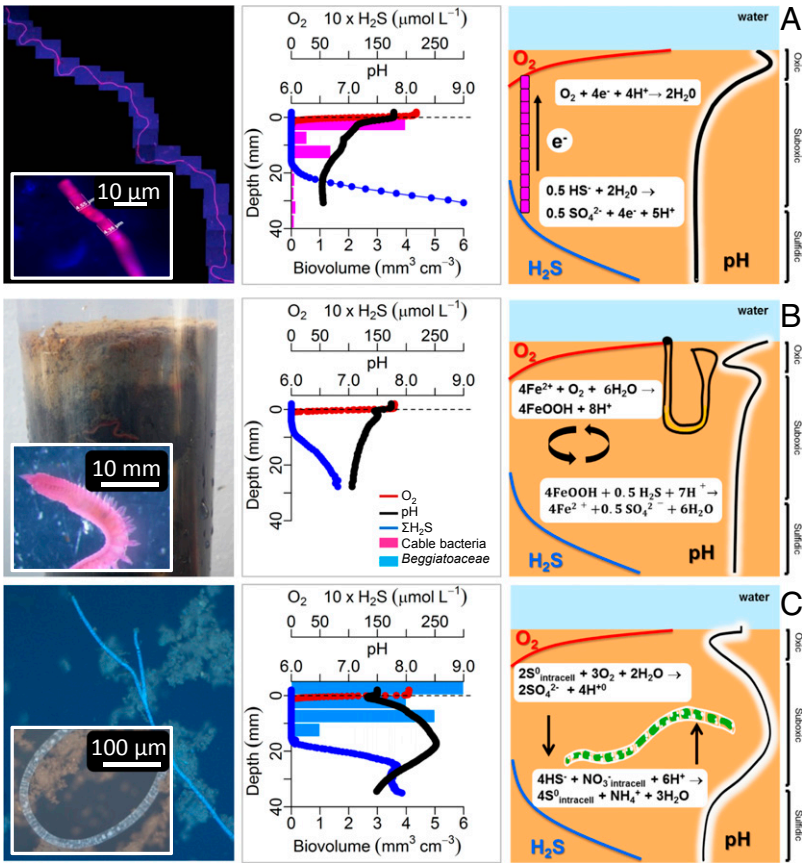

Fig. 2. Three mechanisms of suboxic zone formation were active during 2012 at the study site. (*A*) FISH image of cable bacterium (DSB706 probe) and close-up of a cable bacterium (*Left*); depth profiles of O_2 (in micromoles per liter, red line), pH (black line), and ΣH_2S (in micromoles per liter, blue line) and biovolume (in cubic millimeters per square centimeter) of cable bacteria (pink bar) in March (*Middle*); and schematic representation of geochemical signature and e-SOx carried out by cable bacteria (*Right*). (*B*) Sediment core picture and microscope picture of the polychaete *Scoloplos armiger* (*Left*); microsensor depth profiles in May (*Middle*); and schematic view of effect of the macrofauna on sedimentary iron and sulfur cycling (*Right*). (*C*) *Beggiatoaceae* filament image and close up of a filament (light microscope, stained with DAPI) (*Left*); microsensor depth profiles and *Beggiatoaceae* biovolume (in cubic millimeters per square centimeter, pink bar) in December (*Middle*); and schematic view of geochemical signature and sulfur oxidation carried out by *Beggiatoaceae* (*Right*). *Scoloplos armiger* image courtesy of Monitoring Task Force (Royal Netherlands Institute for Sea Research).

virtual absence from May to August ($B \leq 0.001$ mm^3·cm^{-2}). In September, a population of thin *Beggiatoaceae* filaments (diameter d: 2.4 µm; mean filament length L: 70 µm; B: 0.08 mm^3·cm^{-2}) was found concentrated right at the O_2–H_2S interface, which likely catalyzed the direct aerobic oxidation of free sulfide. Laboratory studies have estimated that sulfide oxidation at the oxic–anoxic interface by *Beggiatoaceae* may be up to 3 times faster than the autocatalytic aerobic chemical oxidation of sulfide (23–25), thus enabling an efficient competition with the abiotic pathway. From October onward, the biovolume of *Beggiatoaceae* filaments drastically increased (B: 2.2–7.5 mm^3·cm^{-2}), and the depth distribution of the *Beggiatoaceae* closely tracked the progressive widening of the suboxic zone (Fig. 2*C*). In addition, the filament diameter and length increased significantly compared with September (*t* test; $n = 672$, $P < 0.001$, regarding both length and diameter), suggesting that a different population of *Beggiatoaceae* was active in late fall that had a metabolism based on intracellular nitrate respiration. Bacterial cell-lysing experiments confirmed that the large *Beggiatoaceae* filaments observed at the field site were storing nitrate into intracellular vacuoles (Fig. S4 and *Supporting Information*).

The pH typology analysis predicted that suboxic zone in May and June was no longer formed by cable bacteria but that metal cycling caused the separation of O_2 and H_2S horizons in the upper first centimeter of the sediment (Fig. 2*B*). This coincided with a sharp rise in the abundance and diversity of the macrofauna in the surface sediment (Fig. 1*D*), suggesting that bioturbation could provide the sediment mixing needed to sustain the metal cycling. An alternative explanation would be that mixing via sediment resuspension is specifically intense during May and June, which is unlikely, however, as meteorological conditions at the field site are typically calm in early summer. With the onset of hypoxia in late June, the macrofauna vanished abruptly, and the sediment remained devoid of macrofauna until December, when recolonization started, although population densities remained low throughout winter. Upon recolonization in spring, the fauna was dominated by small polychaetes and juvenile bivalves, which only have a shallow burrowing depth, consistent with the limited suboxic zone of 7–9 mm observed in May and June. Because fauna are highly sensitive to free sulfide (9–11), the deep removal of sulfide by cable bacteria in early spring may have promoted faunal recolonization.

Microbial Competition for Reduced Sulfur Compounds. In MLG, we observed that cable bacteria were dominant throughout spring, whereas sulfur oxidation was largely carried out by nitrate-accumulating *Beggiatoaceae* throughout fall. This pattern was not only observed in 2012, when detailed monthly sampling was conducted, but was confirmed by seasonal surveys over the period 2011–2015 (Fig. 3 and *Supporting Information*). Combining microsensor profiling and pH-signature analysis, we found that the geochemical signature of cable bacteria is significantly more present in spring, whereas the activity of *Beggiatoaceae* is more likely encountered in fall (Fig. 3). For example, in spring 2015, all sampled sediment sites below 15 m water depth showed the cable bacteria signature, whereas, in fall 2011 and 2014, all sediment revealed the geochemical signature of nitrate accumulating *Beggiatoaceae*. This implies that two distinct types of filamentous S-oxidizing bacteria were competing for the same geochemical niche, but that each type was competitively successful during a distinct period of the year.

The development of *Beggiatoaceae* after summer suggests a better survival of the anoxic period, which could be due to the use of nitrate as an alternative electron acceptor to oxygen. Although both cable bacteria (26) and *Beggiatoaceae* (19–22) can use nitrate for respiration, cable bacteria reach lower population densities when nitrate is the sole electron acceptor (26). Moreover, the nitrate concentration in the bottom water was low (< 1.7 µM) during summer (Fig. S1*B*), and thus, nitrate reduction was likely

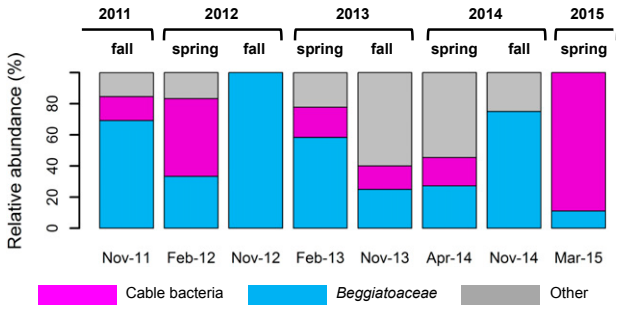

Fig. 3. Relative abundance of the dominant sulfur oxidation pathways carried out by cable bacteria (pink bar), *Beggiatoaceae* (blue bar), and other processes (gray bar) during each fall and spring from November 2011 to March 2015. The geochemical signature (characteristic depth profiles of O_2, pH, and H_2S recorded by microsensor profiling) was used to determine the dominant pathway of sulfur oxidation at any given time at different sites within MLG (*Supporting Information*).

insignificant in sustaining microbial metabolism during anoxia. However, nitrate accumulation before anoxia could have played a role. Presently, there are no indications that cable bacteria can accumulate electron acceptors, whereas *Beggiatoaceae* can store nitrate in intracellular vacuoles (19–22, 25), which can be used as an electron acceptor reservoir to survive the summer period of low bottom water oxygenation (25).

Our seasonal surveys indicate that cable bacteria replace the *Beggiatoaceae* population in winter, yet the reasons for this population switch are not fully understood. One intriguing question is how cable bacteria can "invade" a sediment where a suboxic zone is already established by *Beggiatoaceae*, as recent laboratory experiments show that cable bacteria filaments progressively extend downward from an initial overlap of oxygen and sulfide near the sediment–water interface (27–29). A preexisting suboxic zone thus poses a barrier for sediment colonization by cable bacteria. Future research should hence clarify the drivers and controls of what appears to be a yearly recurrent, and hence predictable, switch between two groups of filamentous S-oxidizing bacteria.

Impact of Cable Bacteria on Geochemistry. Cable bacteria and nitrate-accumulating *Beggiatoaceae* are both capable of efficient sulfide oxidation leading to the creation of a wide suboxic zone. Hence, with regard to biogeochemical cycling in seasonally hypoxic basins, one could ask to what extent it matters whether one or the other is the dominant sulfur oxidizing microbial population? Solid-phase data collected at the field site reveal a notable difference in the iron mineral phases between spring and fall (Fig. 4*A*), and suggest that cable bacteria induce a strong seasonal iron cycling. In March, when cable bacteria were active, a strong depletion of Acid Volatile Sulfides (AVS, interpreted to be mostly iron monosulfides, FeS) occurred in the suboxic zone (11.9 ± 7.3 μmol·S·g^{-1} over the first 3.3 cm; Fig. 4*A*), compared with high values in November (117.0 ± 26.4 μmol·S·g^{-1} over the first 3.3 cm; Fig. 4*A*), when nitrate-accumulating *Beggiatoaceae* were abundant. Exactly the opposite trend was seen in the extractable iron (hydr)oxides (FeOOH), which showed a much higher accumulation in spring (163 ± 52 μmol·Fe·g^{-1}; Fig. 4*A*) than in fall (99 ± 27 μmol·Fe·g^{-1}). Together with our microsensor and microscopy data, these solid-phase data suggest the following seasonal iron cycle (Fig. 4*B*): (*i*) conversion of FeS to FeOOH in spring by cable bacteria; (*ii*) the downward mixing of the FeOOH-rich surface sediment layer in late spring by the newly colonizing fauna, thus enhancing the observed S oxidation by metal oxide reduction; (*iii*) the conversion of FeOOH back to FeS when free sulfide rises to the sediment–water interface during the summer hypoxia period; and (*iv*) the persistence of an FeS pool in the suboxic zone during fall when nitrate-accumulating bacteria are active. Alternative mechanisms, such as winter resuspension events or a strong sedimentation of allochtonous iron (hydr)oxides in winter, cannot suitably explain the observed conversion of FeS to FeOOH in spring (*Supporting Information*). Accordingly, we conclude that observed seasonal iron cycling is principally driven by the FeOOH-forming activity of cable bacteria in spring, and this iron cycle would not occur if nitrate-accumulating *Beggiatoaceae* were dominant throughout the year. Our study therefore demonstrates that not only external environmental factors, such as bottom water oxygen availability, are driving the sedimentary iron and sulfur cycling in seasonally hypoxic basins but that the intrinsic population dynamics of the microbial community, and particularly rapid shifts in sulfur oxidizers, can be equally important.

The metabolic activity of cable bacteria exerts a profound impact on the sediment geochemistry through its effect on pore water pH (15). The electrogenic metabolism induces a spatial uncoupling of sulfide oxidation and oxygen reduction (Fig. 2*A*), and, accordingly, the production and consumption of protons occur widely segregated in space. The establishment of acidic conditions within the deeper suboxic zone promotes the dissolution of iron sulfides, which provides an extra H_2S supply to the cable bacteria in addition to sulfate reduction (16), and the oxidation of this extra H_2S generates more protons, thus establishing a positive feedback (15). In laboratory experiments, it has been shown that FeS dissolution provides up to 40–94% of the sulfide for e-SOx (15, 16), and can completely exhaust the sedimentary FeS pool over a period of weeks (27), while generating a surface enrichment of FeOOH. The observed FeS depletion in the top 4 cm in March shows that cable bacteria also induce strong FeS dissolution in the field, and we speculate that the depletion of the sedimentary FeS stock (Fig. 4*A*) may have limited the electron donor supply, causing the demise of the cable bacteria population in late spring (30).

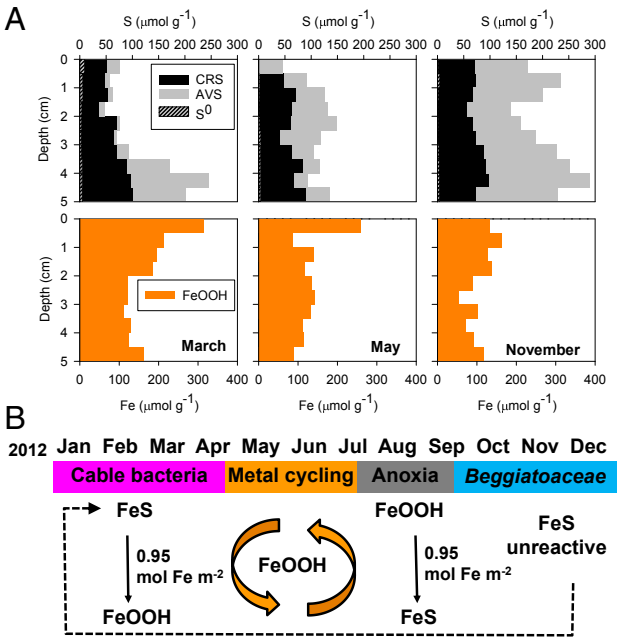

Fig. 4. (*A*) Solid-phase geochemistry in the top 5 cm of the sediment. Depth profiles of S^0, CRS, and AVS (in micromoles S per gram, *Top*) and iron (hydr) oxides (in micromoles Fe per gram, *Bottom*) measured in March (*Left*), May (*Middle*), and November (*Right*). The iron (hydr)oxides represent the total of the nonsulfidized iron. (*B*) Illustration of interconversion between FeS and FeOOH during four time periods in 2012, when the sediment geochemistry was dominated by cable bacteria, metal cycling promoted by sediment mixing, anoxia, and *Beggiatoaceae*.

ECOLOGY

Cable Bacteria in Seasonally Hypoxic Systems and Euxinia. Conventionally, the formation of sulfidic bottom waters is considered to be closely linked to the exhaustion of energetically favorable electron acceptors in the water column, such as oxygen and nitrate (1). Once these electron acceptors are depleted in the bottom water, the oxidation of sulfide in the surface sediment layer is halted, thus enabling a release of sulfide to the overlying water. However, laboratory sediment incubations (31, 32) have previously shown that the disappearance of oxygen and nitrate (anoxia) is not necessarily synchronous with the appearance of free sulfide (euxinia). In sediments that contain a large pool of reactive iron (hydr)oxides before the onset of anoxia, this pool can act as a firewall against the release of free sulfide from the sediment, thus delaying the onset of euxinia (31, 32). Iron (hydr)oxides have a high binding capacity for free sulfide (33); therefore, the efflux of free sulfide only starts after exhaustion of the iron (hydr)oxide pool, which can delay euxinia by several weeks, depending on the size of the initial reactive iron pool (31, 32).

At present, this iron oxide-mediated firewall mechanism has not been demonstrated to occur in seasonally hypoxic basins. Moreover, it is also not expected to occur, as the mechanism requires a yearly buildup of an iron (hydr)oxides pool before the onset of summer anoxia, which is not obvious in seasonally hypoxic environments. Coastal sediments typically accumulate sizeable pools of iron (hydr)oxides only when subjected to strong levels of bioturbation by infauna (34). The ventilation of macrofaunal burrows with oxygen-rich overlying water promotes the oxidation of dissolved ferrous iron (Fe^{2+}) in the pore water (35), whereas particle reworking enhances the oxidation of deeply buried iron sulfides by transporting them upward to the oxic zone of the sediment (36). However, as shown here, such large and deep-burrowing fauna are typically absent from seasonally hypoxic sediments, because the yearly recurrent oxygen depletion increases mortality and decreases recruitment success (11, 37). For this reason, the sediments of seasonally hypoxic coastal systems are generally thought to have a low buffer capacity toward the release of free sulfide (38).

Although sampling at monthly resolution is not sufficient to accurately document the magnitude of the time lag, we observed that anoxia did not coincide with euxinia. Even when the bottom water was devoid of oxygen in August, and nitrate was fully depleted, no free sulfide (concentrations were below the detection limit of < 0.2 μM) was detected in the bottom water. Two potential mechanisms could explain this delay in the formation of euxinia relative to anoxia. The presence of a deep suboxic zone before the onset of bottom water anoxia is one potential mechanism. Before free sulfide can escape the sediment, the suboxic zone has to be transiently replenished with free sulfide, either through local production of sulfide via sulfate reduction or via diffusion of sulfide from deeper sediment horizons. As both cable bacteria and *Beggiatoaceae* induce a suboxic zone, they both induce this form of euxinia delay. Analysis of the curvature of the ΣH_2S depth profile provides an estimate of the sulfide production rate of 0.3 $mol{\cdot}H_2S{\cdot}m^{-3}{\cdot}d^{-1}$ within the first 10 cm of sediment, Accordingly, ∼6 d are required for sulfide to accumulate in the suboxic zone up to the ΣH_2S ∼2-mM level observed in August (porosity of 0.9). In reality, this accumulation of sulfide in the suboxic zone will proceed faster, as molecular diffusion also supplies free sulfide from beneath the suboxic zone. Accordingly, the formation of a deep suboxic zone only delays euxinia for a short period, on the order of a few days at most.

The iron oxide-mediated firewall mechanism is a more effective mechanism for H_2S removal, and has been previously shown to delay sulfide effluxes from sediments for a period of weeks (31, 32). Our results show that cable bacteria generated a large pool of reactive iron (hydr)oxides before the onset of summer hypoxia (0.95 $mol{\cdot}Fe{\cdot}m^{-2}$, as calculated from the difference in FeS and FeOOH inventories over 0–4 cm between spring and fall; *Supporting Information*). Given a depth-integrated sulfide production rate of 30 $mmol{\cdot}H_2S{\cdot}m^{-2}{\cdot}d^{-1}$, this iron (hydr)oxide pool could potentially buffer H_2S production up to ∼36 d. This period is considerably longer than the observed period of anoxia at the study site in 2012 (<20 d), and hence may explain the observed absence of bottom water euxinia in August 2012.

Conclusion

Cable bacteria have only recently been discovered (12, 13), and, hence, little is known about their ecology, life cycle, and natural distribution. Our results demonstrate that cable bacteria can have a major impact on sedimentary biogeochemical cycling in a seasonally hypoxic basin, with potential basin-scale impacts on water column chemistry. In a first report on the occurrence of cable bacteria under natural conditions, it was demonstrated that cable bacteria thrive globally in a wide range of marine sediment habitats, such as coastal mud plains and salt marshes, but that they particularly seem abundant in seasonally hypoxic basins (14). If cable bacteria in other coastal systems follow a similar seasonal cycle to that of MLG, the iron oxide firewall mechanism proposed here could be widely prevalent, and may explain the relatively rare reports of euxinia in coastal systems affected by seasonal hypoxia. However, to accurately document the magnitude and efficiency of this buffer mechanism, a comparison of the sediment geochemistry and microbiology is needed across multiple seasonally hypoxic systems at a higher-than-monthly resolution. Such investigations are crucial, given that seasonal hypoxia in coastal areas is increasing worldwide due to anthropogenic nutrient input and climate change (1).

Materials and Methods

Sampling. We performed monthly sampling campaigns on the R/V *Luctor* in 2012, in the seasonally hypoxic MLG (39). Investigations took place in the Den Osse basin, a deep gully located in the southwestern part of the lake (maximum water depth 34 m; 51.747°N, 3.890°E), and we examined the water column chemistry and sediment biogeochemical processes. Discrete bottom water samples were collected with a 12-L Niskin bottle to assess the O_2 and H_2S concentrations. Water samples from the Niskin bottle were collected via gas-tight Tygon tubing. Bottom water oxygen concentrations were measured using an automated Winkler titration procedure with potentiometric end-point detection (Mettler Toledo DL50 titrator and a platinum redox electrode). Bottom water ΣH_2S concentrations were determined spectrophotometrically (40). Intact sediment cores (6 cm Ø) were retrieved with a UWITEC gravity corer in triplicates. All cores were inspected on retrieval, and only undisturbed cores were used for measurements. Immediately after collection, sediment cores were transported to a nearby laboratory, where microprofiling was started within 2 h of collection and conducted under climate-controlled conditions (temperature of in situ bottom water).

Microsensor Profiling. Microsensor profiling was performed using commercial microelectrodes (Unisense A.S.) for O_2 (25- or 50-μm tip; Unisense), pH (200-μm tip diameter), and H_2S (50-μm tip diameter). Oxygen microprofiles were made at 25- to 50-μm resolution, with a two-point calibration made in air-saturated seawater (100% saturation) and at depth in anoxic sediment (0% saturation). For H_2S and pH, depth profiles were made at 200-μm resolution in the oxic zone, and 400- or 600-μm resolution below. Calibrations for pH were made with three National Bureau of Standards (NBS) standards and a Tris buffer to correct for salinity effects, and pH is reported on the total scale. For H_2S, a five-point calibration was made using Na_2S standards. Total free sulfide ($\Sigma H_2S = H_2S + HS^-$) was calculated from H_2S based on pH measured at the same depth using the R package AquaEnv (41). The OPD is operationally defined as the depth below which $[O_2] < 1$ μM, and the sulfide appearance depth (SAD) is operationally defined as the depth below which $[H_2S] > 1$ μM. The diffusive oxygen uptake (DOU) was calculated from the oxygen depth profiles as in ref. 14.

Pore Water and Solid-Phase Geochemistry. Pore water was extracted from the sediment using centrifugation (15 min at 4,500 × g) and was filtered (0.45 μm) and subsampled under N_2. Centrifuged pore water was subsampled for sulfide, where samples were fixed with zinc acetate and stored at 4 °C. Sulfide was measured spectrophotometrically (40). Centrifuged sediment samples were freeze-dried, then ground in an N_2-purged glove box. Sediment sulfur fractions were separated using the extraction described in ref. 42, and modified as in ref. 43 to include an extraction step for elemental

sulfur. AVS and chromium reducible sulfide (CRS) were quantified using iodometric titration. Solid-phase Fe phases were also extracted and separated according to ref. 44, where Fe oxides were measured as the total of the nonsulfidized Fe pools.

Microscopy. *Beggiatoaceae* filaments were identified via inverted light microscope (Olympus IM) within 24 h of retrieval. Intact sediment cores were sectioned at 5-mm intervals over the top 4 cm from which subsamples (20–30 mg) were used to count living *Beggiatoaceae* filaments. The biovolume was determined by measuring length (10×) and width (40×) of all filaments found in the subsample, according to ref. 45. Microscopic identification of cable bacteria was achieved by FISH, using a *Desulfobulbaceae*-specific oligonucleotide probe (DSB706; 5′-ACC CGT ATT CCT CCC GAT-3′), according to Schauer et al. (27). The depth distribution of cable bacteria was quantified in March, May, August, and November 2012. Cable bacteria biovolume per unit of sediment volume (in cubic millimeters per cubic centimeter) was calculated based on measured filament length and diameter, as well as the areal biovolume of cable bacteria (in cubic millimeters per square centimeter) by depth integration over all eight sediment layers. For macrofauna analysis, sediment collected from eight cores (for a total surface area of ∼0.02 m^2) was wet-sieved (mesh size 1.0 mm) on board. Subsequently, macrofauna were carefully handpicked and preserved in 4% (vol/vol) formalin solution stained with rose bengal. All individuals were identified to species level, where possible, using a stereomicroscope (Leica MZ16), and macrofauna abundance (individuals per square meter) was calculated.

ACKNOWLEDGMENTS. We are grateful to P. van Rijswijk, M. Hagens, A. Tramper, and the crew of the R/V *Luctor* (P. Coomans and M. Kristalijn) for their support during the sampling campaigns. We thank D. Vasquez-Cardenas, H. T. S. Boschker, J. S. Geelhoed, J. J. Middelburg, and M. Hagens for valuable discussions, and E. Zetsche for graphical support. This research was financially supported by the Darwin Center for Biogeosciences (D.S. and F.S.-G.), European Research Council (Grant 306933 to F.J.R.M. and Grant 278364 to C.P.S.), The Netherlands Organisation for Scientific Research (Grant 864.08.004 to F.J.R.M.), and the Danish Council for Independent Research Natural Sciences (R.S.).

1. Middelburg JJ, Levin LA (2009) Coastal hypoxia and sediment biogeochemistry. *Biogeosciences* 6:1273–1293.
2. Jørgensen BB, Fossing H, Wirsen CO, Jannasch HW (1991) Sulfide oxidation in the anoxic Black Sea chemocline. *Deep Sea Res A* 38:S1083–S1103.
3. Thamdrup B, Canfield DE, Ferdelman TG, Glud RN, Gundersen JK (1996) A biogeochemical survey of the anoxic basin Golfo Dulce, Costa Rica. *Rev Biol Trop* 44: 19–33.
4. Turner RE, Rabalais NN, Justic D (2008) Gulf of Mexico hypoxia: Alternate states and a legacy. *Environ Sci Technol* 42(7):2323–2327.
5. Kemp WM, Testa JM, Conley DJ, Gilbert D, Hagy JD (2009) Temporal responses of coastal hypoxia to nutrient loading and physical controls. *Biogeosciences* 6:2985–3008.
6. Conley DJ, et al. (2009) Hypoxia-related processes in the Baltic Sea. *Environ Sci Technol* 43(10):3412–3420.
7. Zhang J, et al. (2010) Natural and human-induced hypoxia and consequences for coastal areas: Synthesis and future development. *Biogeosciences* 7:1443–1467.
8. Ekau W, Auel H, Pörtner HO, Gilbert D (2010) Impacts of hypoxia on the structure and processes in pelagic communities (zooplankton, macro-invertebrates and fish). *Biogeosciences* 7:1669–1699.
9. Vaquer-Sunyer R, Duarte CM (2008) Thresholds of hypoxia for marine biodiversity. *Proc Natl Acad Sci USA* 105(40):15452–15457.
10. Diaz RJ, Rosenberg R (1995) Marine benthic hypoxia: A review of its ecological effects and the behavioural responses of benthic macrofauna. *Oceanogr Mar Biol Annu Rev* 33:245–303.
11. Levin LA, et al. (2009) Effects of natural and human-induced hypoxia on coastal benthos. *Biogeosciences* 6:2063–2098.
12. Nielsen LP, Risgaard-Petersen N, Fossing H, Christensen PB, Sayama M (2010) Electric currents couple spatially separated biogeochemical processes in marine sediment. *Nature* 463(7284):1071–1074.
13. Pfeffer C, et al. (2012) Filamentous bacteria transport electrons over centimetre distances. *Nature* 491(7423):218–221.
14. Malkin SY, et al. (2014) Natural occurrence of microbial sulphur oxidation by long-range electron transport in the seafloor. *ISME J* 8(9):1843–1854.
15. Meysman FJR, Risgaard-Petersen N, Malkin SY, Nielsen LP (2015) The geochemical fingerprint of microbial long-distance electron transport in the seafloor. *Geochim Cosmochim Acta* 152:122–142.
16. Risgaard-Petersen N, Revil A, Meister P, Nielsen LP (2012) Sulfur, iron-, and calcium cycling associated with natural electric currents running through marine sediment. *Geochim Cosmochim Acta* 92:1–13.
17. Aller RC, Rude PD (1988) Complete oxidation of solid phase sulfides by manganese and bacteria in anoxic marine sediments. *Geochim Cosmochim Acta* 52:751–765.
18. Canfield DE, et al. (1993) Pathways of organic carbon oxidation in three continental margin sediments. *Mar Geol* 113:27–40.
19. Mussmann M, et al. (2003) Phylogeny and distribution of nitrate-storing *Beggiatoa* spp. in coastal marine sediments. *Environ Microbiol* 5(6):523–533.
20. Sayama M, Risgaard-Petersen N, Nielsen LP, Fossing H, Christensen PB (2005) Impact of bacterial NO_3^- transport on sediment biogeochemistry. *Appl Environ Microbiol* 71(11):7575–7577.
21. Lichtschlag A, Felden J, Bru V (2010) Geochemical processes and chemosynthetic primary production in different thiotrophic mats of the Hakon Mosby Mud Volcano (Barents Sea). *Limnol Oceanogr* 55(2):931–949.
22. Preisler A, et al. (2007) Biological and chemical sulfide oxidation in a Beggiatoa inhabited marine sediment. *ISME J* 1:341–353.
23. Jørgensen BB, Revsbech NP (1983) Colorless sulfur bacteria, *Beggiatoa* spp. and *Thiovulum* spp., in O_2 and H_2S microgradients. *Appl Environ Microbiol* 45(4):1261–1270.
24. Jørgensen BB, Postgate JR (1982) Ecology of the bacteria of the sulphur cycle with special reference to anoxic–oxic interface environments. *Philos Trans R Soc Lond B Biol Sci* 298(1093):543–561.
25. Schulz HN, Jørgensen BB (2001) Big bacteria. *Annu Rev Microbiol* 55:105–137.
26. Marzocchi U, et al. (2014) Electric coupling between distant nitrate reduction and sulfide oxidation in marine sediment. *ISME J* 8(8):1682–1690.
27. Schauer R, et al. (2014) Succession of cable bacteria and electric currents in marine sediment. *ISME J* 8(6):1314–1322.
28. Larsen S, Nielsen LP, Schramm A (2015) Cable bacteria associated with long-distance electron transport in New England salt marsh sediment. *Environ Microbiol Rep* 7(2): 175–179.
29. Vasquez-Cardenas D, et al. (2015) Microbial carbon metabolism associated with electrogenic sulphur oxidation in coastal sediments. *ISME J* 9(9):1966–1978.
30. Nielsen LP, Risgaard-Petersen N (2015) Rethinking sediment biogeochemistry after the discovery of electric currents. *Annu Rev Mar Sci* 7:425–442.
31. Kristensen E, Kristiansen KD, Jensen MH (2003) Temporal behavior of manganese and iron in a sandy coastal sediment exposed to water column anoxia. *Estuaries* 26(3): 690–699.
32. Kristiansen KD, Kristensen E, Jensen MH (2002) The influence of water column hypoxia on the behaviour of manganase and iron in sandy coastal marine sediment. *Estuar Coast Shelf Sci* 55:645–654.
33. Rozan TF, et al. (2002) Iron-sulfur-phosphorus cycling in the sediments of a shallow coastal bay: Implications for sediment nutrient release and benthic macroalgal blooms. *Limnol Oceanogr* 47(5):1346–1354.
34. Kristensen E, Kostka JE (2005) Macrofaunal burrows and irrigation in marine sediment: Microbiological and biogeochemical interactions. *Interactions Between Macro-Microorganisms in Marine Sediments*, eds Kristensen, Kostka JE, Haese R (Am Geophys Union, Washington, DC), pp 125–157.
35. Aller RC (2001) *The Benthic Boundary Layer: Transport Processes and Biogeochemistry* (Oxford Univ Press, Oxford), pp 269–301.
36. Meysman FJR, Middelburg JJ, Heip CHR (2006) Bioturbation: A fresh look at Darwin's last idea. *Trends Ecol Evol* 21(12):688–695.
37. Rosenberg R, Agrenius S, Hellman B, Nilsson HC, Norling K (2002) Recovery of marine benthic habitats and fauna in a Swedish fjord following improved oxygen conditions. *Mar Ecol Prog Ser* 234:43–53.
38. Jørgensen BB, Nelson DC (2004) Sulfur oxidation in marine sediments: Geochemistry meets microbiology. *Sulfur Biogeochemistry—Past and Present*, eds Amend JP, Edwards KJ, Lyons TW (Geol Soc Am, Boulder, CO), pp 63–81.
39. Hagens M, et al. (2015) Biogeochemical processes and buffering capacity concurrently affect acidification in a seasonally hypoxic coastal marine basin. *Biogeosciences* 12: 1561–1583.
40. Cline J (1969) Spectrophotometric determination of hydrogen sulfide in natural waters. *Limnol Oceanogr* 14(3):454–458.
41. Hofmann AF, Soetaert K, Middelburg JJ, Meysman FJR (2010) AquaEnv: An aquatic acid-base modelling environment in R. *Aquat Geochem* 16:507–546.
42. Burton ED, Sullivan LA, Bush RT, Johnston SG, Keene AF (2008) A simple and inexpensive chromium-reducible sulfur method for acid-sulfate soils. *Appl Geochem* 23: 2759–2766.
43. Kraal P, Burton ED, Bush RT (2013) Iron monosulfide accumulation and pyrite formation in eutrophic estuarine sediments. *Geochim Cosmochim Acta* 122:75–88.
44. Poulton SW, Canfield DE (2005) Development of a sequential extraction procedure for iron: Implications for iron partitioning in continentally derived particulates. *Chem Geol* 214:209–221.
45. Jørgensen BB, Dunker R, Grünke S, Røy H (2010) Filamentous sulfur bacteria, *Beggiatoa* spp., in arctic marine sediments (Svalbard, 79°N). *FEMS Microbiol Ecol* 73(3): 500–513.
46. Canfield DE (1993) The anaerobic degradation of organic matter in Danish coastal sediments: iron reduction, manganese reduction, and sulfate reduction. *Geochim Cosmochim Acta* 57(16):3867–3883.
47. Thamdrup B, Fossing H, Jørgensen BB (1994) Manganese, iron and sulfur cycling in a coastal marine sediment, Aarhus bay, Denmark. *Geochim Cosmochim Acta* 58(23): 5115–5129.
48. Thamdrup B, Rosselló-Mora R, Amann R (2000) Microbial manganese and sulfate reduction in Black Sea shelf sediments. *Appl Environ Microbiol* 66(7):2888–2897.
49. Jourabchi P, Van Cappellen P, Regnier P (2005) Quantitative interpretation of pH distributions in aquatic sediments: A reaction-transport modeling approach. *Am J Sci* 305:919–956.

Supporting Information

Seitaj et al. 10.1073/pnas.1510152112

SI Results and Discussion

Study Site Description and Seasonal Water Column Chemistry. MLG (surface area 115 km^2) is a former estuary in the Delta region, in the southwest of The Netherlands. In 1971, this water body was closed off from the North Sea by a dam, turning the estuary into a marine lake, which consists of separate basins. Most areas of the impoundment are shallow, consisting of <12.5 m water depth. Due to limited water exchange with the open sea, water column stratification develops each summer, leading to seasonal hypoxia in the bottom waters of the deeper basins (Fig. S1). A comprehensive overview of stratification and the water circulation in MLG is given in ref. 39.

Water column temperature and salinity data were used to calculate the stratification parameter ϕ (in joules per cubic meter) (Fig. S1), which is defined as the amount of energy required to fully homogenize the water column through vertical mixing (39),

$$\phi = \frac{1}{H}\int_{-H}^{0}(\rho_{av}-\rho w)gzdz \quad \text{where} \quad \rho_{av} = \frac{1}{H}\int_{-H}^{0}\rho w\, zdz,$$

where H is the total height of the water column (in meters), z is depth (in meters), g is gravitational acceleration (in meters per square second), ρ_w is water density (in kilograms per cubic meter), and ρ_{av} is the average water column density (in kilograms per cubic meter).

Sulfur Cycling Budget. The sulfate reduction rate (SRR) was estimated from the production and accumulation of total free sulfide ($\Sigma H_2S = [HS^-] + [H_2S]$) in the first 10 cm of the sediment (Fig. S2). The production rate of free sulfide was estimated as the upward flux toward the bottom of the suboxic zone, as calculated from Fick's first law $J = -\varphi\, D_s\, dC/dx$, where $\varphi = 0.89$ is the local porosity, D_s is the effective diffusion coefficient in the pore water, and dC/dx is the concentration gradient (obtained by linear regression of the ΣH_2S depth profile). The effective diffusion coefficient was calculated as $D_s = D_{mol}/\theta^2$, where we assume that bisulfide (HS^-) is the dominant pore water species and the molecular diffusion coefficient D_{mol} was calculated from the CRAN:marelac package as a function of temperature and salinity. A tortuosity correction $\theta^2 = 1–2\ln(\varphi)$ was implemented. Note that this approach does not account for the local sulfate reduction within the suboxic zone, and, hence, it provides a conservative estimate for SRR. The monthly SRR varied between 4 $mmol{\cdot}S{\cdot}m^{-2}{\cdot}d^{-1}$ and 30 $mmol{\cdot}S{\cdot}m^{-2}{\cdot}d^{-1}$ over the year 2012, and reached a maximum of 30 $mmol{\cdot}S{\cdot}m^{-2}{\cdot}d^{-1}$ in August, with an annual average of 10.7 $mmol{\cdot}S{\cdot}m^{-2}{\cdot}d^{-1}$ or 3.9 $mol{\cdot}S{\cdot}m^{-2}{\cdot}y^{-1}$. The DOU at the study site was calculated in a similar way by applying Fick's first law to the oxygen depth profile just below the sediment–water interface. The monthly DOU varied between 16.9 $mmol{\cdot}O_2{\cdot}m^{-2}{\cdot}d^{-1}$ and 58.1 $mmol{\cdot}O_2{\cdot}m^{-2}{\cdot}d^{-1}$, with an annual average of 23.6 $mmol{\cdot}O_2{\cdot}m^{-2}{\cdot}d^{-1}$ or 8.6 $mol{\cdot}O_2{\cdot}m^{-2}{\cdot}y^{-1}$.

The burial of reduced sulfur compounds was estimated from the concentrations of iron sulfides ([FeS] determined as AVS: 0.15 $mmol{\cdot}S{\cdot}g^{-1}$ dry sediment) and pyrite ([FeS_2] determined as CRS: 0.12 $mmol{\cdot}S{\cdot}g^{-1}$ dry sediment) at 10 cm depth. The burial rate was calculated as $F = (1-\varphi)\, w\, \rho\, ([FeS] + [FeS_2]) = 1.1\ mol{\cdot}S{\cdot}m^{-2}{\cdot}y^{-1}$, where $\varphi = 0.9$ is the porosity at 10 cm depth, w is the burial velocity [2 $cm{\cdot}y^{-1}$ as determined by Pb^{210} radionuclide dating (14)], and ρ is the solid-phase density (2.6 $g{\cdot}cm^{-3}$). Using an average SRR of 10.7 $mmol{\cdot}m^{-2}{\cdot}d^{-1}$, we found that 39% of the free sulfide produced is buried as iron sulfides or pyrite.

Accordingly, the remaining ~61% of the sulfide production (2.4 $mol{\cdot}S{\cdot}m^{-2}{\cdot}y^{-1}$) must be reoxidized to sulfate, if no free sulfide escapes the sediment. If oxygen is the sole terminal electron acceptor ($H_2S + 2O_2 \rightarrow SO_4^{2-} + 2H^+$), one needs 2 mol of oxygen per mole of sulfide, and so the required oxygen consumption rate (4.8 $mol{\cdot}S{\cdot}m^{-2}{\cdot}y^{-1}$) is smaller than the calculated DOU of the sediment. If sulfide reoxidation occurred solely by nitrate-accumulating *Beggiatoaceae*, the reoxidation of sulfide occurs in two steps: the oxidation of H_2S to S^0 by nitrate and the intracellular storage of S^0 (upon migration of *Beggiatoaceae* into the deeper suboxic zone) and then the oxidation of intracellular S^0 to sulfate by oxygen (upon migration to the oxic layer at the surface). This process ($S^0 + 3/2O_2 + H_2O \rightarrow SO_4^{2-} + 2H^+$) predicts an overall oxygen consumption of 3.6 $mol{\cdot}O_2{\cdot}m^{-2}{\cdot}y^{-1}$, which is below the observed DOU.

pH Typology and Seasonal Succession of Sulfur Cycling Pathways. To determine which sulfur oxidation mechanisms were active through the seasonal cycle, we developed a pH signature typology. Different sulfur oxidation pathways will release and consume protons (or more exactly, alkalinity) within different sediment horizons, and, hence, they will induce a specific pH depth profile in the pore water. This way, the pH depth profile (in combination with the O_2 and H_2S depth profiles) provides a characteristic signature of the sulfur oxidation mechanism at hand. Below, we discuss five types of pH profiles, which each could be associated with a specific form of sulfur cycling. In this way, microsensor depth profiling allows screening of which sulfur cycling pathways are active throughout the year (Fig. 1*C* and Fig. S3), and, as discussed in the text, this reveals a rapid temporal succession of different sulfur cycling pathways at the field site.

e-SOx by cable bacteria. The electrogenic metabolism of cable bacteria induces a distinct geochemical signature in the interstitial pore water (Fig. 2*A*), which is characterized by strong pH excursions (12, 15, 27). High proton consumption occurs within the shallow oxic zone due to cathodic oxygen reduction ($O2 + 4e^- + 4H^+ \rightarrow 2H_2O$), creating a pH maximum near the OPD. Similarly, proton production takes place within the deeper part of the suboxic zone due to anodic sulfide oxidation ($1/2\ H_2S + 2H_2O \rightarrow 1/2\ SO_4^{2-} + 4e^- + 5H^+$), which generates a pH minimum at depth. This characteristic e-SOx signature (26) was recorded by microsensor profiling in January (Fig. S3) and February, when pH depth profiles showed a narrow maximum within the oxic zone (8.04 ± 0.21 pH units in January and February) accompanied by a broad pH minimum near the SAD (pH 6.37 ± 0.17 below 20 mm depth; Fig. 2). In March, no subsurface pH peak was detected, but acidic conditions (6.49 ± 0.13 pH units) persisted at 25–30 mm depth, and FISH data confirmed a dense population of cable bacteria present (Fig. 1*D*). Reactive transport simulations have recently shown that at high e-SOx rates, the subsurface pH maximum shifts toward the sediment–water interface and becomes less pronounced, making it more challenging to detect by microsensor profiling (15). In April, the pH within the suboxic zone (6.84 ± 0.08) remained below 7, which we used as an operational threshold for e-SOx activity, but the pH depth profile was less characteristic and showed signs of a transition toward another sulfide oxidation regime.

Sulfur oxidation through iron cycling. The cycling of iron between reduced and oxidized forms requires solid-phase mixing, which transports oxidized forms (FeOOH) into deeper sulfidic layers and brings up reduced forms of iron (e.g., FeS, Fe^{2+} adsorbed onto solids) toward oxic surface layer (46, 47). As a result of this,

protons are produced in the oxic zone (e.g., $Fe^{2+} + 1/4\ O_2 + 3/2H_2O \rightarrow FeOOH + 2H^+$), leading to a pH minimum near the OPD where reoxidation takes place, and, similarly, protons are produced in deeper layers (e.g., $4FeOOH + 1/2\ HS^- + 8H^+ \rightarrow 4Fe^{2+} + 1/2\ SO_4^{2-} + 6H_2O$), leading to a subsurface pH increase. In reality, the redox pathways can be more complex, as there can be multiple parallel transport pathways of iron transport, as well as an intermediate cycle of manganese between iron and oxygen (48). However, overall, iron cycling leads to release of protons within the oxic surface layer and consumption of protons in the deeper suboxic zone, as confirmed by reaction transport modeling of pH distributions in marine sediments (49). This geochemical signature of metal cycling in the surface sediment was observed in the microsensor profiles recorded in May 2012 (Fig. S3). Although the FISH data show that cable bacteria maintained a dense population in May, the pH depth distribution (Fig. S3) suggests that e-SOx was no longer as dominant in May. Compared with January–March, the pH in the suboxic zone evolved toward more alkaline values, increasing from 6.84 ± 0.08 in April to 7.26 ± 0.07 in June (Fig. 1*C*). Rather than a pH maximum, the pH depth profile in May showed a subsurface minimum (7.57) at the OPD, followed by a small pH increase (7.63) and subsequent decrease (7.18) at 26 mm depth (Fig. 2). The pH profiles recorded in June were similar to those in May, and, hence, the period of metal cycling, as indicated by the pH typology, coincided with the higher abundances of macrofauna (Fig. 1*D*), which may have generated the required solid-phase mixing through bioturbation.

Summer anoxia. The establishment of low-oxygen conditions (28.8 μmol·L^{-1}, 11% air saturation) in the bottom water in July resulted in a clear change in the pH depth profile. The pH decreased to around 7.3 ± 0.1 pH units over the first 5 mm and subsequently remained constant with depth (Fig. S3), while the sulfide horizon migrated upward and the sulfide depth profile switched from convex to concave. This geochemical signature suggests the production of sulfide through sulfate reduction at depth and an upward transport by molecular diffusion (15). The pH depth profile did not exhibit the subsurface maximum but showed a monotonous decrease, which is the expected profile when sulfate reduction is the dominant mineralization pathway. Sulfate reduction ($2CH_2O + SO_4^{2-} \rightarrow 2HCO_3^- + H_2S$) releases dissolved inorganic carbon and alkalinity in equal proportions, which explains the gradual decrease in pH with depth.

Canonical sulfur oxidation at the O_2–H_2S interface. Right after the reoxygenation of the bottom waters in September, oxygen and free sulfide showed a small overlap, allowing canonical sulfur oxidation to occur (i.e., the direct redox interaction of H_2S and O_2 as defined in ref. 15). The pH profile that was recorded is consistent with recent reactive transport model simulations (14), showing a monotonous decrease with depth. The pH decreased in the narrow oxic zone (~7.73) down to the oxic–anoxic interface (~7.41), where the oxidation of sulfide releases protons (e.g., $HS^- + 2\ O_2 \rightarrow SO_4^{2-} + H^+$). In deeper anoxic layers, the pH became constant with depth (~7.19 below 5 mm depth), and thus stabilized at slightly lower values compared with August.

***Sulfur oxidation by nitrate-accumulating* Beggiatoaceae.** In fall, the sediment was characterized by yet another type of geochemical signature (Fig. 2*C*), which suggested that another pathway of sulfide oxidation was dominant. In the period from October to December, the pH depth profiles showed a distinct sigmoid shape, with a subsurface minimum located at the OPD that became progressively pronounced (from 7.52 ± 0.06 to 7.28 ± 0.04), and increasingly alkaline near the sulfide horizon (from 7.79 ± 0.10 to 8.48 ± 0.05). The sigmoid pH depth profile has been previously linked to the metabolism of motile, nitrate-respiring *Beggiatoaceae* (18, 19), and reflects the proton production/consumption associated with spatial separation of the two sequential steps in sulfide oxidation (Fig. 2*C*). The oxidation of sulfide at depth via intracellular nitrate ($4HS^- + {NO_3^-}_{intracell} + 6H^+ \rightarrow 4{S^0}_{intracell} + NH_4^+ + 3H_2O$) consumes protons, thus explaining the broad pH maximum at the sulfide horizon. The elemental sulfur (S^0) generated from this oxidation is stored intracellularly, and once the gliding *Beggiatoaceae* reach the oxic zone, elemental sulfur is further oxidized to sulfate using oxygen as the electron acceptor ($2{S^0}_{intracell} + 3O_2 + 2H_2O \rightarrow 2SO_4^{2-} + 4H^+$). This latter reaction produces protons, and therefore induces a pH minimum near the OPD (Fig. 2*C*).

Interconversion of FeS and FeOOH. The depletion of the FeS pool (as shown by the AVS depth profiles) in the uppermost 3.5 cm and accumulation of iron (hydr)oxides in the first 2 cm of sediment in spring suggests conversion of FeS to FeOOH (Fig. 4*B*). We attribute this to dissolution of FeS ($FeS + H^+ \rightarrow Fe^{2+} + HS^-$) by the acid-generating metabolism of the cable bacteria, followed by aerobic oxidation of ferrous iron in the oxic surface sediment ($4Fe^{2+} + O_2 + 6H_2O \rightarrow 4FeOOH + 8H^+$). By fall, these iron (hydr)oxides have been converted again to FeS, as seen by the increase FeS pool and a decrease in the pool of extractable iron (hydr)oxides (Fig. 4*B*). We attribute this interconversion to the reduction iron (hydr)oxides by free sulfide under anoxic conditions in summer ($8FeOOH + 9HS^- + 7H^+ \rightarrow 8FeS + SO_4^{2-} + 12H_2O$). The resulting conversion was quantified by calculating the change in the inventory $I = \int_0^L \rho_s(1-\phi)C(x)dx$ of both AVS and extractable Fe oxides between March and November 2012. In this, ρ_s is the solid-phase density (2.60 g·cm^{-3}), ϕ represents porosity, $C(x)$ is the measured concentration depth profile (in micromoles per gram), and L = 4 cm is the integration depth (i.e., the depth horizon affected by metabolic FeS dissolution of cable bacteria). The calculated increase in the AVS inventory amounted to 1.17 mol·Fe·m^{-2}, and the observed decrease in FeOOH inventory was 0.73 mol·Fe·m^{-2}. Given the uncertainties associated with the operational extraction procedures for these iron phases, this suggests a nearly stoichiometric interconversion of ~0.95 mol·Fe·m^{-2} (the mean of both values) from FeOOH into FeS over the summer period.

Nitrate Accumulation in *Beggiatoaceae* Filaments. *Beggiatoaceae* filaments were identified by microscopy based on size, motility, and the presence of sulfur inclusions. To verify that the large *Beggiatoaceae* filaments observed at the field site were capable of nitrate accumulation, and hence nitrate respiration, lysis experiments were conducted as described in ref. 19. Two intact sediment cores were sliced from 0 cm to 2 cm at depth intervals of 0.2 mm, and, beyond this, every 0.5 cm down to 3 cm. The samples were stored frozen (−20 °C) for several weeks, to allow the lysis of any nitrate accumulating cells. Pore water was separated by centrifugation of thawed sediment samples at 3,000 × g for 10 min, and the nitrate concentration was determined in the supernatant by using standard colorimetric method on a Seal QuAAtro autoanalyzer. Nitrate was present in the pore water at high concentrations throughout the suboxic zone, with a maximum of 374 ± 64 μmol·L^{-1} near the surface and gradually decreasing to 8 ± 1 μmol·L^{-1} at 3 cm depth (Fig. S3). These pore water concentrations strongly exceeded the bottom water nitrate concentrations (7.1 μmol·L^{-1}), suggesting that the nitrate was likely contained in intracellular vacuoles of the *Beggiatoaceae*.

In addition, the nitrate accumulation was measured in individual hand-picked *Beggiatoaceae* filaments. Around 40 *Beggiatoaceae* filaments (~10–20 μm diameter) were separately picked using a glass needle, transferred to vials with 0.25 mL of demineralized water, and immediately frozen at −20 °C. Nitrate was measured in the supernatant after thawing and centrifugation, as described above. The bacterial biovolume was calculated based on the average measured diameter (15 μm) and assuming a filament length of 70 μm. Based on this estimated biovolume of filaments, and assuming that 80% of the cell consists of vacuoles, the average vacuolar nitrate concentrations was 51 ± 23 mmol·L^{-1}. This concentration is slightly lower compared with previous observations in

Beggiatoceae in coastal sediments, reporting intracellular nitrate concentrations of 73–390 mmol·L^{-1} (19, 22, 43).

Multiyear Survey of Sulfur Oxidation Pathways. The relative presence of sulfur oxidation pathways was surveyed each spring and fall over a time span of 4 y, i.e., from November 2011 to March 2015. Sampling campaigns were performed at multiple locations (three to six sites, always including the current field site) within the deeper basins of MLG (sediments of >15 m water depth subject to seasonal hypoxia; see Fig. S1*A*). The dominant sulfur oxidation pathways were determined based on the pH typology (Fig. S3), which was confirmed by detailed microscopic observations in a systematic fashion throughout the monthly samplings throughout 2012 at the field site (as noted in *pH Typology and Seasonal Succession of Sulfur Cycling Pathways*). Three intact sediment cores were collected per site and were used for microsensor profiling (O_2, pH, and H_2S). Each set of microsensor depth profiles was classified into one of three categories: (category 1) e-SOx by cable bacteria as (Fig. 2*A*); (category 2) sulfur oxidation by nitrate-accumulating *Beggiatoaceae* (Fig. 2*B*); and (category 3) "other," which contained microsensor depth profiles that did not unambiguously fit the categories 1 or 2. Note that only profiles which had a clear signature were classified in categories 1 and 2, and so, when uncertain, the profile set was attributed to category 3. The relative abundance of sulfur oxidation pathways was calculated as the percentage of each category recorded during each campaign (Fig. 3).

Ruling Out Alternative Mechanisms of FeS to FeOOH Conversion. The depletion of the FeS pool in the uppermost 3.5 cm and concurrent accumulation of iron (hydr)oxides sediment in spring suggests that a conversion of FeS to FeOOH has taken place. As already noted above, we attribute this conversion to dissolution of FeS by the acid-generating metabolism of the cable bacteria, followed by aerobic oxidation of ferrous iron in the oxic surface sediment. We now examine the likelihood of two alternative mechanisms for FeOOH accumulation in the surface sediment in winter.

Storm-induced resuspension events in winter. If a resuspension event occurred, then any FeS in the surface sediment layer would be suspended in an oxic water column and could be oxidized to FeOOH. However, there are two arguments that speak against this mechanism. Firstly, if a resuspension event caused the FeS to FeOOH oxidation, then, after settling, the FeOOH formed would be uniformly distributed over the depth horizon over which FeS is depleted (~3.5 cm). However, our data show no such uniform FeOOH distribution with depth, but rather a local accumulation of FeOOH right at the sediment surface. The latter observation is hence not consistent with resuspension, but is consistent with the colonization depth of cable bacteria. The FeS to FeOOH hence is driven by dissolution of FeS by cable bacteria, subsequent diffusion of Fe^{2+} to the oxic zone, and oxidation and reprecipitation of FeOOH near the sediment. Secondly, these resuspension events cannot explain the observed growth of a dense cable bacteria population. If an FeOOH-rich surface layer was already present before the presence of the cable bacteria, the development of cable bacteria would likely be hampered, as there would no longer be a source of free sulfide (their primary electron donor). Previous studies have shown that FeS dissolution and sulfate reduction are the two sources of sulfide for the e-SOx metabolism (16). If the sediment fully consists of FeOOH, it is difficult to perform e-SOx, as there is no FeS reservoir to dissolve, and no sulfate reduction ongoing (as dissimilatory iron conduction would outcompete sulfate reduction).

Strong seasonal sedimentation of allochtonous iron oxides. Given the strong accumulation of sediment at the field site, there is clearly a flux of mineral iron to the sediment jointly with other detrital matter. MLG is closed off from river input by a dam, and hence receives no significant input of terrigeneous matter. However, MLG is in communication with the open sea via a sluice, which allows the exchange of water with the North Sea (39). Hence, the high sedimentation rates are explained by lateral input of detrital matter from the adjacent North Sea, which then settles in the more quiescent MLG, and accumulates in the deeper basins through local sediment focusing. However, seasonality in the deposition of iron minerals cannot explain the observed depth distributions of FeS and FeOOH. If deposition were the driver, rather than the oxidation of FeS to FeOOH, then a strong difference in the composition of settling particles between spring (low FeS, high FeOOH) and fall (high FeS, low FeOOH) would be required. However, in both seasons, the water column is oxygenated, and, therefore, strong differences in the composition of settling particles are unlikely. Moreover, the depth profiles of suspended matter in the water column showed no seasonality throughout 2012, which rules out strong seasonality in sedimentation. Secondly, the depth layer affected by the switch between FeOOH and FeS extends down to 3.5 cm, which far exceeds the accumulation depth over the 6 mo between November and March (<1 cm). In conclusion, we contend that deposition or depositional changes cannot explain the observed depth distributions of FeS and FeOOH.

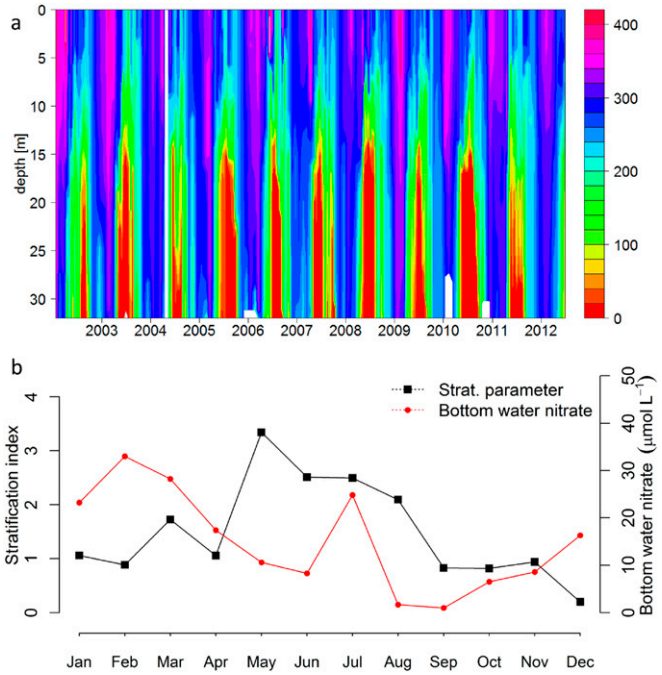

Fig. S1. (*A*) Oxygen concentrations (micromoles per liter) recorded over the period 2002–2012 show a regular pattern of seasonal hypoxia in the deeper bottom waters at the MLG field site. Data collected by Rijkswaterstaat (Dutch Ministry of Infrastructure and the Environment). (*B*) Bottom water nitrate concentrations (micromoles per liter, red circles) and stratification index (joules per cubic meter, black squares) as recorded in monthly sampling campaigns throughout 2012.

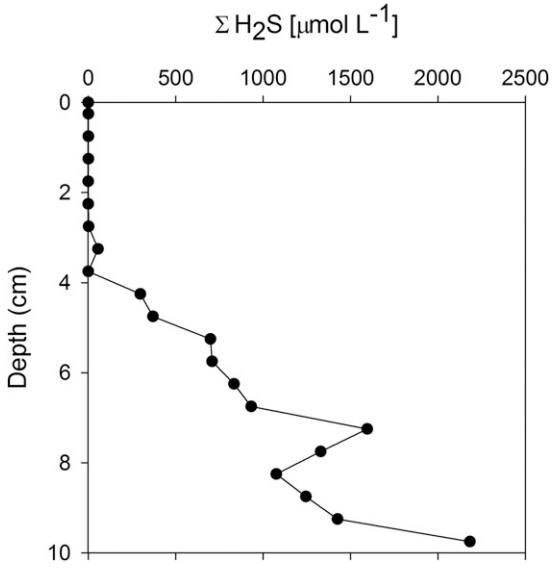

Fig. S2. Sulfide concentrations in the pore water in the upper 10 cm of sediment in January. Pore water samples were obtained upon sediment centrifugation.

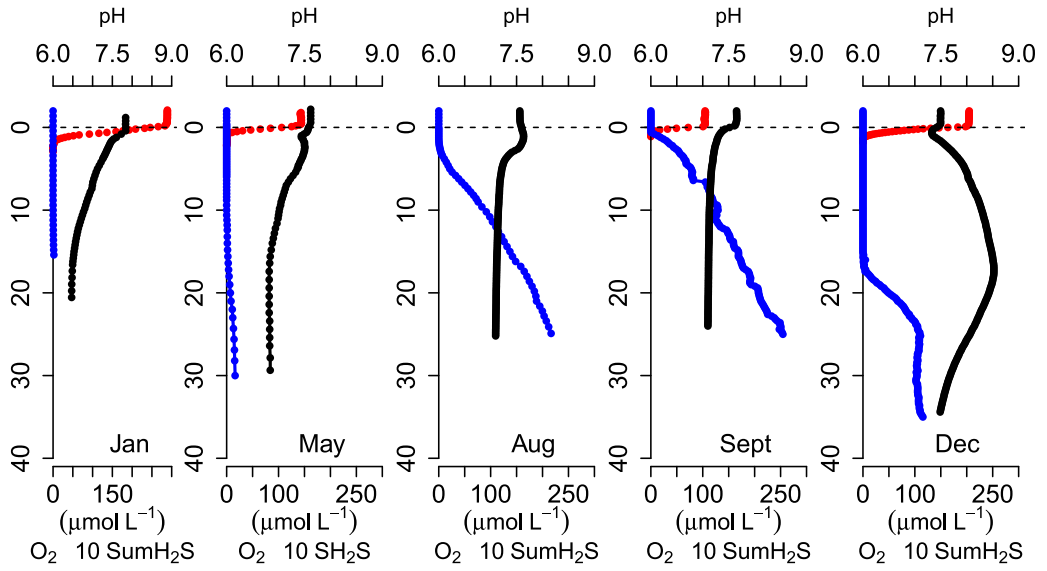

Fig. S3. Pore water depth profiles of O_2 (red line), pH (black line), and ΣH_2S (blue line) at the filed site in January, May, August, September, and December. These so-called geochemical signatures illustrate the different types of sulfur cycling that were active at the field site.

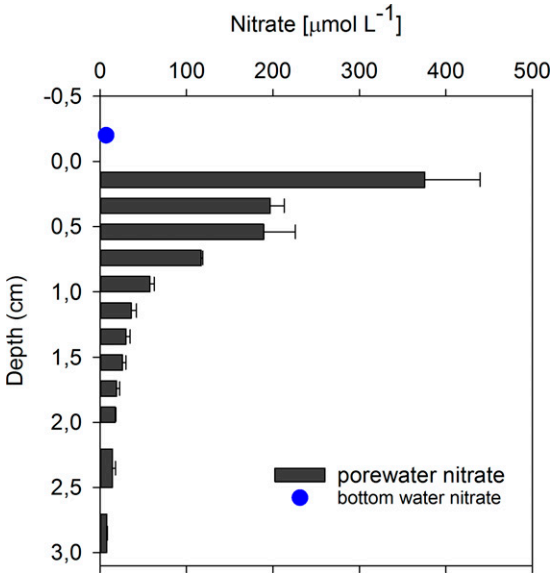

Fig. S4. Nitrate concentrations (dark gray bars) in the pore water after lysis of nitrate-accumulating cells, during *Beggiatoaceae* dominance. The nitrate concentrations in the pore water were substantially (up to ~50 times) higher than in the overlying water (blue dot), suggesting intracellular nitrate accumulation by *Beggiatoaceae*.